# Local structure of a trapped photoexcited state of a Fe-Co cyanide studied by x-ray-absorption fine-structure spectroscopy

Toshihiko Yokoyama, Manabu Kiguchi, and Toshiaki Ohta
*Department of Chemistry, Graduate School of Science, The University of Tokyo, 7-3-1 Hongo, Bunkyo-ku, Tokyo 113-0033, Japan*

Osamu Sato
*Kanagawa Academy of Science and Technology, Tokyo Institute of Polytechnics, 1583 Iiyama, Atsugi, Kanagawa 243-0213, Japan*

Yasuaki Einaga
*Department of Applied Chemistry, Graduate School of Engineering, The Univerity of Tokyo, 7-3-1 Hongo, Bunkyo-ku, Tokyo 113-0033, Japan*

Kazuhito Hashimoto
*Kanagawa Academy of Science and Technology, Tokyo Institute of Polytechnics, 1583 Iiyama, Atsugi, Kanagawa 243-0213, Japan and Research Center for Advanced Science and Technology, The University of Tokyo, 4-6-1 Komaba, Meguro-ku, Tokyo 153-0041, Japan*

(Received 16 March 1999; revised manuscript received 14 May 1999)

The local structure of a trapped photoexcited state of a Fe-Co cyanide magnetic material, $Na_{0.4}Co_{1.3}Fe(CN)_6 \cdot 5H_2O$, was investigated by Fe and Co *K*-edge x-ray-absorption fine-structure spectroscopy. The excited state was prepared by visible-light irradiation at 36 K. In order to obtain detailed structural information, temperature dependence of the local structure was also studied without light irradiation. The Fe-C distance shows almost no change by light irradiation (1.92 Å before and after irradiation), while the average Co-N/O distance is noticeably elongated (1.94 and 2.08 Å before and after irradiation, respectively). This phase transformation is caused by the charge transfer from the $Fe^{II}(S=0)$-CN-$Co^{III}(S=0)$ configuration to $Fe^{III}(S=1/2)$-CN-$Co^{II}(S=3/2)$. The local structure of the trapped photoexcited state was found to be identical with that of the high-temperature phase, although the high-temperature phase was created much more effectively by light irradiation than thermal activation. [S0163-1829(99)00637-2]

## I. INTRODUCTION

Prussian blue analogs have recently attracted great interest because of their various characteristics as molecular magnets. It is especially emphasized that magnetic properties of prussian blue analogs can be modified easily by substituting and/or mixing various transition metal ions such as V, Cr, Mn, Fe, Co, and Ni. High critical temperatures ($T_c$) have been reported; for instance $T_c=315$ K for $V[Cr(CN)_6]_{0.86} \cdot 2.8H_2O$ (air sensitive)[1] and $T_c=270$ K for $Cr_{2.12}(CN)_6$ (air stable).[2] These $T_c$ values are in the highest region among the molecular-based magnets that have ever been prepared to date. On the other hand, Sato *et al.*[3] discovered the induction of a magnetic phase transition in Fe-Co cyanides by optical stimuli. Although both $Na_{0.4}Co_{1.3}Fe(CN)_6$ and $K_{0.4}Co_{1.3}Fe(CN)_6$ are paramagnetic down to 2 K, they become ferrimagnets upon visible-light (500–750 nm) irradiation. Up to ~100 K, the ferrimagnetic behavior is preserved. Moreover, upon irradiation of near-infrared light (1319 nm), the phases turn back to the paramagnetic ones.

Structural information on the prussian blue analogs is quite important to understand these interesting magnetic properties. Since it is very difficult or impossible to prepare single crystalline samples for x-ray-diffraction measurements, x-ray-absorption fine-structure (XAFS) spectroscopy is useful. We have recently performed Fe and Co *K*-edge XAFS analyses of several Fe-Co cyanide systems at 30 and 296 K.[6] Here, the electronic states of Fe and Co strongly depend on temperature as well as the material. In the previous study, the Co(II):Co(III) composition ratios for various Fe-Co cyanides which is dependent on temperature were quantitatively determined by the factor analysis[7] of the XANES (x-ray-absorption near-edge structure) spectra. The local structures were also elucidated by the EXAFS (extended x-ray-absorption fine-structure) spectroscopy.

The property of light-induced ferrimagnetization mentioned above is also quite attractive. The Na and K salts of the Fe-Co cyanides exhibit the magnetic phase transitions. At low temperature the electronic configuration of Fe(II) and Co(III) is stable, while at high temperature the Fe(III)-Co(II) configuration is dominated due to larger entropy.[3,4,6] When the sample is irradiated by visible lights at low temperature, the photoexcited state is trapped and shows ferrimagnetism. The trapped state is stable up to ~100 K.[3] In the present study, we have investigated the electronic and local atomic strcutures of $Na_{0.4}Co_{1.3}Fe(CN)_6 \cdot 5H_2O$ after visible-light irradiation at 36 K by means of XAFS spectroscopy. Structural and electronic changes have also been studied by heating the irradiated sample to higher temperatures. Although quantitative structure determination of photoexcited states is seriously limited because of the lifetimes, the present system can well be trapped at low temperature and thus be suitable for structure studies of photoexcited states by means of

 

XAFS spectroscopy. Moreover, in the present study, temperature dependence of the XAFS spectra was investigated in detail without light irradiation in order to compare the local structure of the trapped photoexcited state with those of the low- and high-temperature phases.

## II. EXPERIMENTAL

$Na_{0.4}Co_{1.3}Fe(CN)_6 \cdot 5H_2O$ was prepared electrochemically. Details of the sample preparation is described elsewhere.[4] Fe and Co *K*-edge XAFS spectra of the Co-Fe cyanide were taken in the conventional transmission mode at the Beamlines 7C and 10B of the Photon Factory (operation energy of 2.5 GeV and stored current of 400–200 mA) at the Institute of Materials Structure Science.[9,10] Si(111) double crystals (the first crystals were cooled with water) were employed as a monochromator without focusing. In order to reduce higher-order harmonics, the double crystals were detuned by around ~40%. No mirrors were inserted in the present setup. The intensities of the incident and transmitted x rays were recorded using ionization chambers filled with $N_2$.

For the temperature dependent XAFS measurements at the Beamline 10B, the sample was diluted with BN and pressed to prepare a disk (diameter of 12 mm). The Fe *K*-edge jump was estimated to be 0.45, while the maximum total absorption coefficient was less than 3.0, this implying less importance of the higher-harmonics contribution. For the XAFS measurements at 36–300 K, a closed-cycle He refrigerator was employed, while for the higher-temperature measurements (300–360 K), a simple electric furnace was used. Typical data acquisition time was 1 s/point for XANES and 2 s/point for EXAFS, and we recorded 21 Co *K*-edge and 11 Fe *K*-edge XAFS spectra for the temperature range of 36–360 K.

For the experiment of visible-light irradiation at the Beamline 7C, the sample was not diluted with BN but dispersed on a Scotch tape in order to make the sample as transparent as possible for the visible-light irradiation. The resultant Fe *K*-edge jump was only 0.03, which was much smaller than the one for the temperature-dependent measurements, indicating worse signal-to-noise ratios.

The sample was first cooled down to 36 K and the Fe and Co *K*-edge XANES spectra were recorded. Subsequently the sample was irradiated by visible lights from a halogen lamp for 30 min. In order to avoid a temperature rise during irradiation, an Al foil was inserted between the sample holder and the Scotch tape. A small amount of Fe *K*-edge jump from impurities in the Al foil was observed (10% of the edge jump of the sample). Thus the Fe *K*-edge spectra from the sample were resultantly obtained by subtracting the one from the Al foil only. The data acquisition period was 2 s/point for XANES and 4 s/point for EXAFS. The present irradiation time of 30 min should be long enough to obtain sufficiently saturated concentration of the photoexcited states since the spectral features irradiated for 5 min was found to be identical to those for 30 min. The photoexcited state was stable completely during the XAFS measurements.

In order to observe the phase transformation, the irradiated sample at 36 K was heated up to 150 and 300 K, and the spectral changes of Fe and Co *K*-edge XANES were finally investigated. It is noted that no detectable creation of the trapped photoexcited state by x rays was seen in any measurement. This was confirmed by our temperature-dependent measurements where at low-temperature regions no meaningful changes were observed among continual XANES scans. This is quite reasonable since the absorption cross section for x rays is several orders of magnitude smaller than that for visible lights.

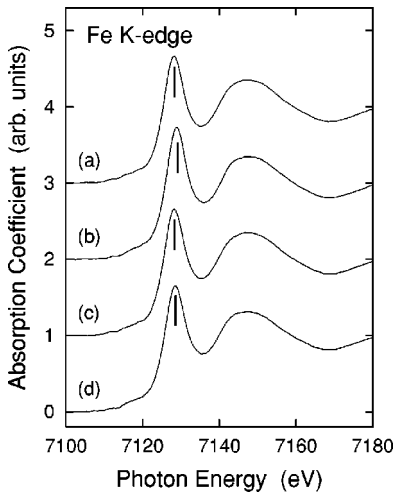


FIG. 1. Experimental Fe *K*-edge XANES spectra in the sequential visible-light irradiation experiments: (a) before irradiation at 36 K, (b) after irradiation at 36 K, (c) heating the irradiated sample to 150 K, and (d) subsequent heating to 300 K. In the Fe *K*-edge spectra, the position of the first resonance is indicated by a vertical line to see the energy shift more clearly.

## III. RESULTS OF XANES

### A. XANES

Figures 1 and 2 shows, respectively, the Fe and Co *K*-edge XANES spectra for the visible-light irradiation experiment. First of all, let us compare the spectra before irradiation (a) with those at 300 K (d). One can find clear difference in the Co *K*-edge XANES spectra, exemplifying the occurrence of the phase transition, while the Fe *K*-edge XANES spectra look similar to each other. According to the previous studies,[3,5,6] the Fe ions are exclusively divalent at the low-temperature limit. This implies that the composition ratio of Co(III) is 76.9% within the accuracy of the elemental analysis. Both the Fe(II) and Co(III) ions are in the low-spin states of $(3dt_{2g})^6(3de_g)^0$ $(S=0)$, while the minor Co(II) ions (23.1%) are in the high-spin state of $(3dt_{2g})^4(3de_g)^3$ $(S=3/2)$, which shows paramagnetism. At temperatures higher than ~260 K, the phase transition occurs, which is ascribed to the charge transfer from Fe(II) to Co(III); namely, the $Fe^{II}$-CN-$Co^{III}$ configuration turns to the $Fe^{III}$-CN-$Co^{II}$ one. Here the Fe(III) ions are again in the low-spin state of $(3dt_{2g})^5(3de_g)^0$ $(S=1/2)$, and in the pure high-temperature phase all the Co ions are in the high-spin Co(II) state.

Since the spin state is different between 36 and 300 K for Co, the Co *K*-edge XANES spectra exhibit noticeable change as in Fig. 2. On the other hand, the Fe ions are in the low-spin state irrespective of the Fe valency. Thus the Fe *K*-edge

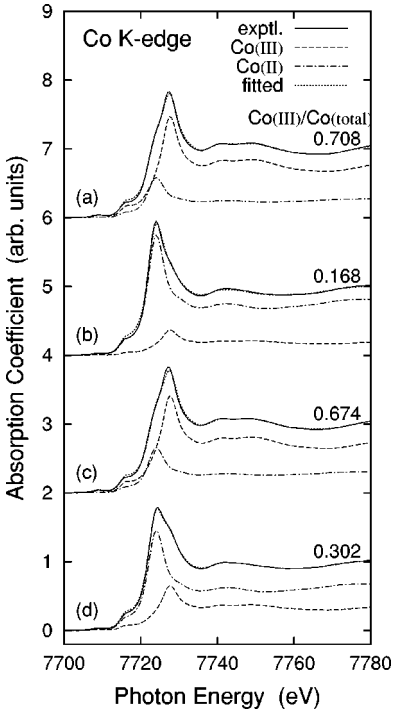


FIG. 2. Experimental Co *K*-edge XANES spectra (solid line) in the sequential visible-light irradiation experiments: (a) before irradiation at 36 K, (b) after irradiation at 36 K, (c) heating the irradiated sample to 150 K, and (d) subsequent heating to 300 K. In the Co *K*-edge spectra, the results of the factor analysis are also given. The Co(III) composition ratio is given numerically, and the estimated pure Co(II) and Co(III) spectra are plotted as dot-dashed and dashed lines, respectively, where the edge jumps correspond to the composition ratios. For further details, see text.

XANES spectra resemble each other. A small edge energy shift to a higher energy side can nevertheless be seen from Fe(II) (36 K) to Fe(III) (300 K), which is indicated by vertical lines at the first resonances in Fig. 1. The first peak-top energies at 36 and 300 K are 7128.2 and 7128.9 eV, respectively (note here that the absolute photon energy was not necessarily calibrated and that only the relative energies should be discussed). On the other hand, those for reference materials $K_4Fe^{II}(CN)_6 \cdot 3H_2O$ and $K_3Fe^{III}(CN)_6$ are, respectively, 7127.9 and 7129.4 eV.[6] A smaller energy shift (0.7 eV vs 1.5 eV) might be reasonable because of mixture of Fe(II) and Fe(III) in the present material both at 36 and 300 K.

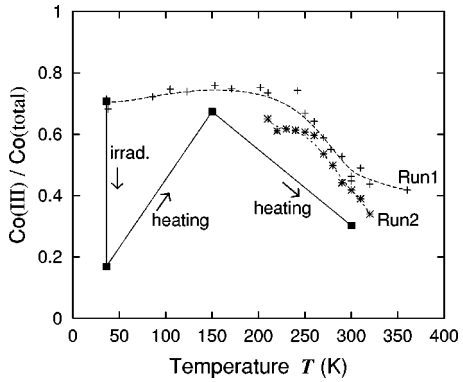


FIG. 3. Temperature dependence of the Co(III) composition ratio. The results of the light-irradiation experiments are also given. For the temperature dependence measurements, two different runs were carried out using independently prepared samples. The irradiated sample was the same as that used in run 2.

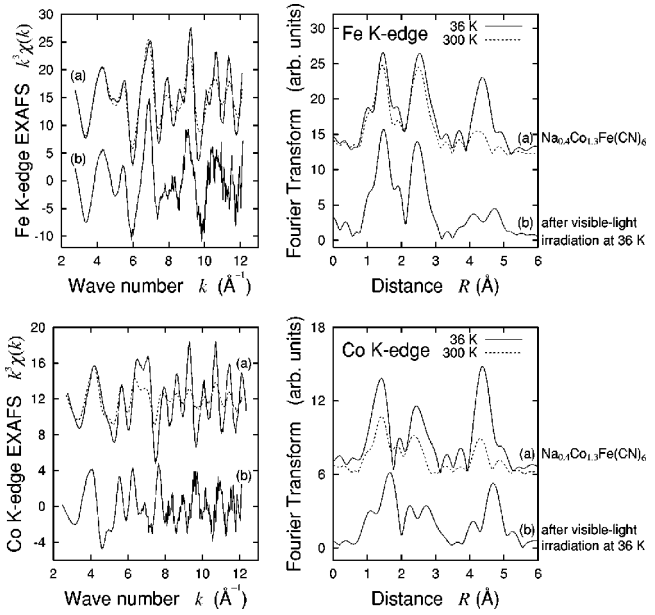


FIG. 4. Fe and Co *K*-edge EXAFS oscillation functions $k^3\chi(k)$ and their Fourier transforms: (a) before irradiation at 36 K (solid line) and at 300 K (dashed line), and (b) after irradiation.

After visible-light irradiation at 36 K, the Co *K*-edge spectrum changes drastically, this clarifying that the trapped excited state was successfully obtained. The spectrum is

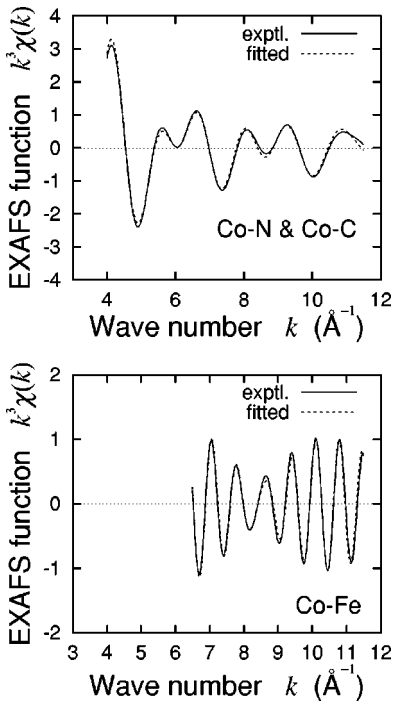


FIG. 5. Examples of the curve-fitting results for the Co *K*-edge EXAFS analysis for the present sample at 300 K. The upper panel gives the results for the Co-N and Co-C four-shell fits, while the lower panel shows those for the Co-Fe two-shell fits. For details, see the text and Ref. 6.

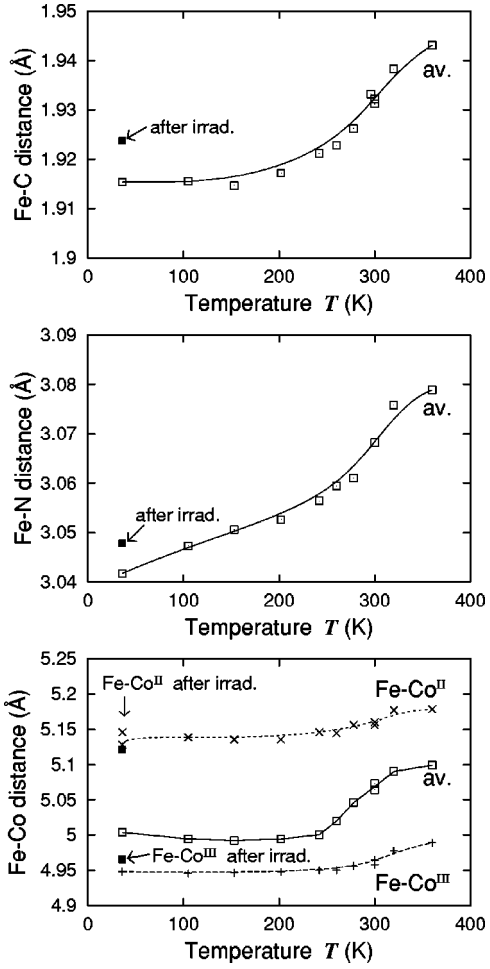


FIG. 6. Temperature dependence of the Fe-C, Fe-N, and Fe-Co distances determined by the Fe *K*-edge EXAFS analysis. For the Fe-Co shell, the average Fe-Co distance is also plotted, together with those of the Fe-Co(II) and Fe-Co(III) ones. Those of the light-irradiated sample are also depicted.

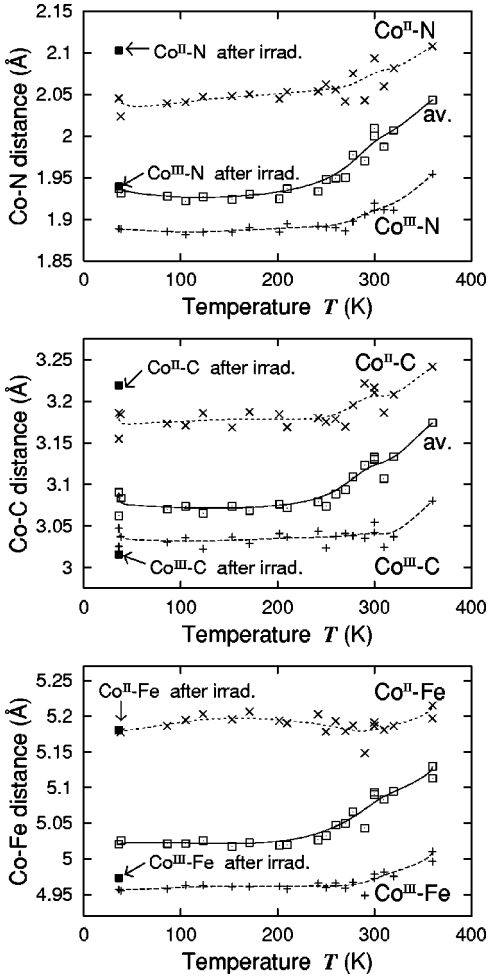


FIG. 7. Temperature dependence of the Co-N(+O), Co-C, and Co-Fe distances determined by the Co *K*-edge EXAFS analysis. The distances of each Co component are plotted, together with those of the light-irradiated sample. The average distances for the temperature dependence are also depicted.

rather similar to that at 300 K, implying that the dominant Co species is in the high-spin Co(II) state. A small edge energy shift in the Fe *K*-edge spectrum was also observed. The first peak top appears at 7129.1 eV, which means the energy shift of 0.9 eV. This is consistent with corresponding change of the Fe valency from Fe(II) to Fe(III). Upon heating the irradiated sample to 150 K, the Co *K*-edge spectra turned back to the low-temperature ones, this implying that the trapped excited state at 36 K is thermally deexcited to the ground state at 150 K. The first peak top in the Fe *K*-edge XANES is seen at 7128.2 eV, which is also identical with that at 36 K. For further heating to 300 K, the sample underwent the phase transition to provide the high-temperature phase.

In our previous study,[6] we found that the Co *K*-edge XANES spectra allow us to estimate the Co(III) composition ratios quantitatively through the factor analysis.[7] In the present analysis, we can employ lots of Co *K*-edge data sets (not shown in figures) which were taken in the temperature-dependent measurements and contain temperature-dependent composition ratios. We have performed a similar factor analysis to obtain the composition ratios and the pure spectra of the Co(II) and Co(III) species. The numerical results in the irradiation experiments are indicated in Fig. 2, and are plotted in Fig. 3, where the temperature-dependent measurements are also included. In Fig. 3, two different results for the temperature dependence are given (run 1 and run 2). The sample employed in the irradiation experiment corresponds to run 2. Although the absolute Co(III) contents are slightly different between run 1 and run 2, the transition temperature seems identical and the reproducibility of the samples and measurements is considered to be satisfactory.

Before irradiation, the Co(III) ratio was found to be 0.708. Although the value seems to be a little smaller than the ideal one for the low-temperature phase (0.769), one can regard the sample as almost the pure low-temperature phase. After irradiation, the Co(III) ratio was reduced to 0.168, which implies that a dominant species is derived from the high-temperature Co(II) phase. After heating of the irradiated sample to 150 K, the Co(III) low-temperature phase recovers almost completely. After heating to 300 K, the thermal phase transition takes place, and the Co(III) ratio is again reduced to 0.302, which means that most Co atoms are in the high-temperature phase.

One can here note that the irradiated sample contains larger amount of the Co(II) high-temperature phase than the

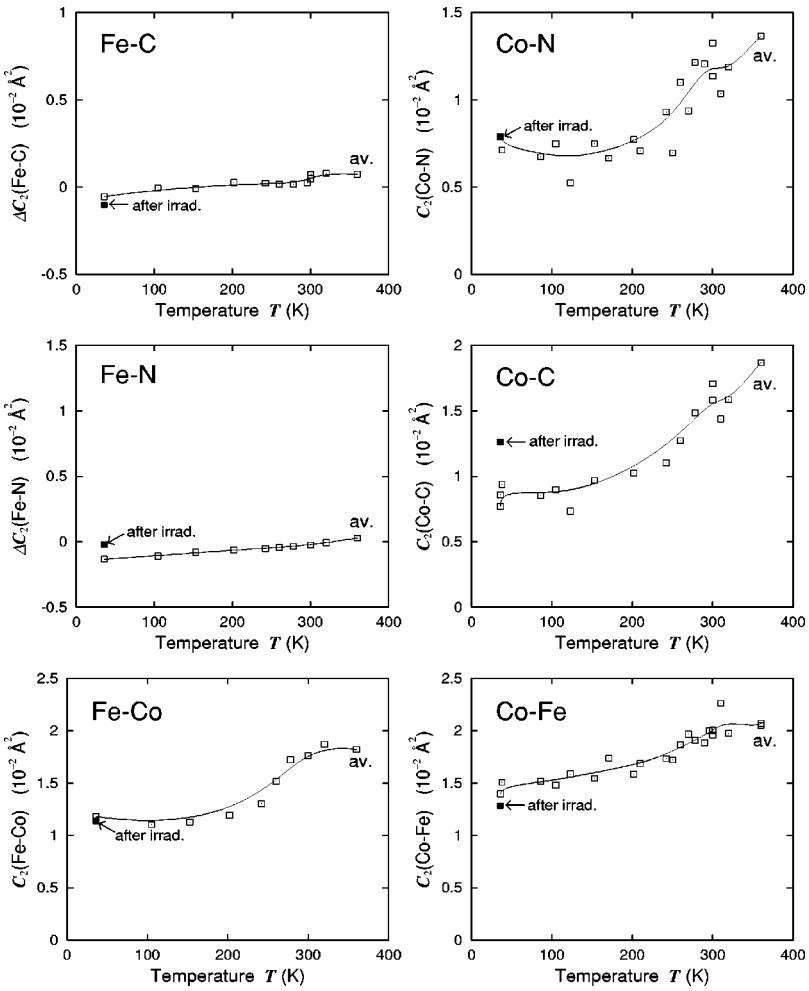


FIG. 8. Temperature dependence of the Fe-C, Fe-N, Fe-Co, Co-N(+O), Co-C, and Co-Fe Debye-Waller factors $C_2$ determined by the Fe and Co *K*-edge EXAFS analysis. Those for Fe-C and Fe-N shells are given as differences with respect to the empirical standard of $K_3Fe^{III}(CN)_6$, while the others are obtained based on the FEFF standards (the absolute values are tentatively given).

sample at 300 K. A small amount of the Co(III) phase was nevertheless observed, although in an ideal case the Co(III) phase should disappear completely. Since the irradiation period was found to be sufficiently long to yield a saturated concentration of the excited state, the presence of a small Co(III) fraction may be caused by more intrinsic origins. Some areas may have a shorter life time. Defects, particle surfaces or crystal water may play a significant role.

### B. EXAFS

The EXAFS analysis was carried out also in a similar manner to our previous paper.[6] The EXAFS oscillation functions $k^3\chi(k)$ were obtained by means of standard analysis procedures: pre-edge baseline subtraction, post-edge background estimation using cubic spline functions and the normalization with the atomic absorption coefficients.[11] Figure 4 shows the EXAFS functions $k^3\chi(k)$ and their Fourier transforms for the irradiated sample at 36 K and the nonirradiated one at 36 and 300 K. The employed $\Delta k$ ranges in the Fourier transforms were 2.8–12.1 ($\text{Å}^{-1}$) for Fe *K*-edge and 2.8–12.2 ($\text{Å}^{-1}$) for Co K edge.

In the Fourier transforms of the Fe *K*-edge EXAFS, one can find three dominant contributions at $\sim$1.4, $\sim$2.5, and $\sim$4.3 Å, which are attributed to the Fe-C, Fe-N, and Fe-Co shells, respectively. Because of a linear configuration of the Fe-C-N-Co chain, the Fe-N and Fe-Co shells are noticeably enhanced due to the multiple-scattering focusing effect. The features of the Fe-C and Fe-N shells among the three spectra (irradiated, 36 and 300 K) do not differ so much from each other, this indicating little structure change of the $Fe(CN)_6$ unit irrespective of the charge difference. On the other hand, the Fe-Co shell exhibits clear temperature difference and the irradiated sample shows a complicated split feature, this indicating significant structural changes around Co.

Drastic changes concerning the local structures around Co are actually observed in the Co *K*-edge EXAFS spectra. In the Fourier transforms of the Co *K*-edge EXAFS, one can again find three dominant contributions at $\sim$1.4–1.7, $\sim$2.5, and $\sim$4.3–4.6 Å, which are assigned to the Co-N/O, Co-C, and Co-Fe shells, respectively. The first shell of Co-N/O implies that the O atom in water molecules is additionally coordinated to make the Co coordination saturated. Since the ionic radii of high-spin Co(II) and low-spin Co(III) are quite different from each other, we should take account of four independent shells of Co(III)-N, Co(II)-N, Co(III)-C, and Co(II)-C in the *R* range of 1–3.3 Å. Due to such a complexity, additional peaks such as a sidelobe at $\sim$2.0 Å for the 36 K spectrum appear strongly.

In order to obtain the interatomic distances, the curve-fitting analysis was performed in *k* space. Details of the fitting procedures are given in our previous report.[6] For the Fe *K*-edge EXAFS spectra, since the ionic radii of Fe(II) and Fe(III) are almost the same (both are in the low-spin states), average distances can be obtained. The analysis of the Fe-C

TABLE I. Interatomic distances of $Na_{0.4}Co_{1.3}Fe(CN)_6 \cdot 5H_2O$ determined by the Fe and Co *K*-edge EXAFS analysis.

| | Co valence | Before irrad. at 36 K | After irrad. at 36 K | Heated at 300 K |
|---|---|---|---|---|
| $Co^{III}$ ratio | | 0.693 | 0.168 | 0.338 |
| Fe-C | | 1.915(10) | 1.924(20) | 1.933(10) |
| Fe-N | | 3.04(2) | 3.05(3) | 3.05(2) |
| Fe-Co | (III) | 4.95(3) | 4.97(4) | 4.98(4) |
| | (II) | 5.13(5) | 5.15(5) | 5.16(5) |
| | av. | 5.00(3) | 5.12(4) | 5.14(4) |
| Co-N/O | (III) | 1.89(1) | 1.94(2) | 1.92(2) |
| | (II) | 2.05(3) | 2.11(3) | 2.11(3) |
| | av. | 1.937(10) | 2.075(20) | 2.044(20) |
| Co-C | (III) | 3.05(3) | 3.02(5) | 3.06(5) |
| | (II) | 3.19(5) | 3.22(5) | 3.22(5) |
| | av. | 3.09(2) | 3.18(3) | 3.17(3) |
| Co-Fe | (III) | 4.98(3) | 4.97(5) | 4.98(5) |
| | (II) | 5.20(5) | 5.18(5) | 5.20(5) |
| | av. | 5.04(3) | 5.14(4) | 5.13(4) |

and Fe-N shells is rather straightforward since each contribution can be separated by the Fourier filtering and a reference material of $K_3Fe(CN)_6$ is available.

On the other hand, the analysis of the Fe-Co shell requires a two-shell fit because the Fe-Co(II) and Fe-Co(III) distances are noticeably different from each other. We already know, however, the Co(II):Co(III) composition ratios through the above factor analysis of Co *K*-edge XANES. Moreover, the coordination numbers can be expected assuming the structure of a prussian blue; the local structure around Fe is $Fe(CN)_6Co_6$ where the subscripts denote the coordination number. Thus if the edge-energy shift $\Delta E_0$ is referred to from the previous work,[6] the fitting parameters are only the distance and the Debye-Waller factor for each shell.

In the case of the Fe-Co shell, four parameters should be fitted, this being rather simple. Here, since no reference spectra are available, the theoretical standards given by FEFF6 (Ref. 8) were employed. In this calculation, a cluster of octahedral $Fe(CN)_6Co_6$ was assumed. There exists a possibility of some local buckling of the Fe-CN-Co chain which was assumed to be collinear in the present analysis. This effect is reported in mixed alkali halides.[12] The previous analysis,[6] however, shows that the average Fe-Co distances obtained agree excellently well with the lattice constants given by the power-diffraction patterns, this indicating that the effect of local buckling could be neglected with a rather high accuracy also in the present photoexcited system.

In the Co *K*-edge EXAFS analysis, since no suitable reference materials can be prepared, the FEFF6 standard was employed assuming a cluster of $Co(NC)_6Fe_6$. Note here that in real systems the local structure around Co is $Co(NC)_{4.61}(H_2O)_{1.39}Fe_{4.61}$ because of different contents of Fe and Co. The present FEFF standard thus implies that the $Co–OH_2$ shell is assumed to be identical to the Co-N shell, this being reasonable because of similar scattering amplitudes between N and O.

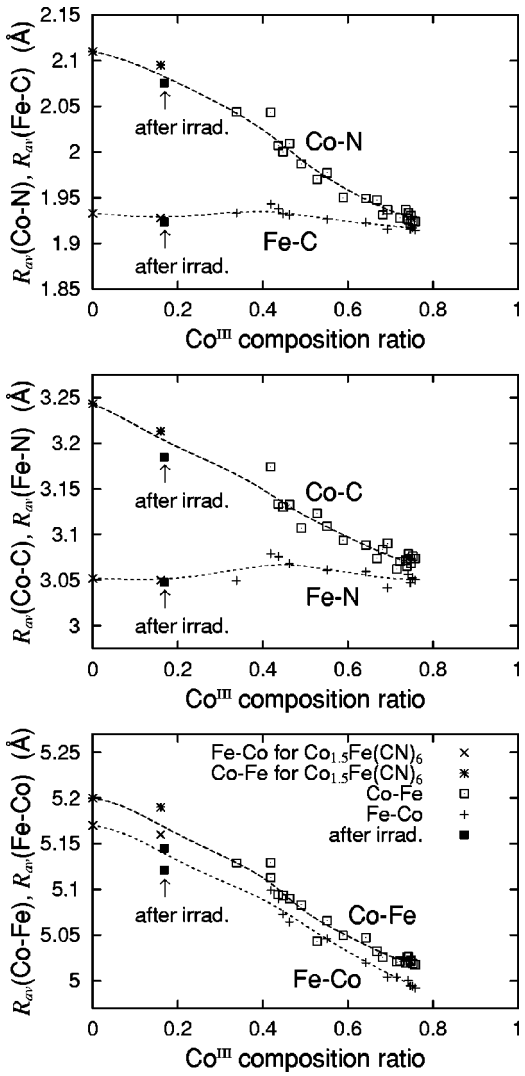


FIG. 9. Average interatomic distances as a function of the Co(III) composition ratio. For comparison, the results of $Co_{1.5}Fe(CN)_6$ are also given (Ref. 6).

The analysis of the Co-N/O and Co-C shells are complicated since there exist four inequivalent contributions of Co(III)-N/O, Co(II)-N/O, Co(III)-C, and Co(II)-C, even when the first-nearest neighbor Co-N and Co-O shells are regarded as identical. This requires eight fitting parameters, each shell containing two parameters of the distance and the Debye-Waller factor. As described in the previous paper,[6] however, reliable results were consequently obtained. In these multishell analyses, reliable analyses could not have been carried out without knowing the the Co(III) composition ratios. Information from the XANES spectra is essential.

The analysis of the Co-Fe shells was performed in a similar manner to that of the Fe-Co shells in the Fe *K*-edge EXAFS. Examples of the fitting results are depicted in Fig. 5 both for the Co-N/O and Co-C four-shell fits and for the Co-Fe two-shell ones of the present material at 300 K. Except for the low-*k* region of the Co-Fe shell (omitted in the fitting procedure and not shown), the agreements between the experimentally extracted spectra and the FEFF-based simulations are satisfactory.

The analyzed results of the interatomic distances are depicted in Figs. 6 and 7 as a function of temperature. Table I

summarizes some numerical values. In order to verify the reliabilities of the interatomic distances, the temperature dependence of the average Debye-Waller factors $C_2$ for all the shells analyzed are also plotted in Fig. 8. For the Fe-C and Fe-N shells, because the interatomic distances are almost the same between Fe(II) and Fe(III), the temperature dependence of $C_2$ is quite small, which originates dominantly from the enhancement of the vibrational amplitude with a temperature rise. On the other hand, those for all the other shells are more temperature dependent because of the additional and more important origin of coexistence of Co(II) and Co(III), whose ionic radii are essentially different from each other (see Fig. 7). Since the temperature dependence of $C_2$ is too complicated to obtain thermal properties of the Co bondings in this material, no quantitative discussion would be necessary for the present purpose.

As observed in Fig. 7, the interatomic distance for each Co component shows less temperature dependence, while the average distances for Co(II) and Co(III) are elongated when temperature exceeds $\sim$200 K because of the increase in the Co(II) composition ratio at high temperature. Although it is hard to compare the results of the irradiated sample with those of temperature dependence, the interatomic distances for each Co component look similar. In order to make it more clearly, the average interatomic distances are plotted as a function of the Co(III) composition ratio. This is shown in Fig. 9. In these plots, the previous results[6] are also included for $Co_{1.5}Fe(CN)_6$, which consists of high-spin Co(II) and low-spin Fe(III) (almost) irrespective of temperature. Although the Fe-Co and Co-Fe distances of the irradiated sample are slightly underestimated, it can be remarked that all the average distances are on the dashed lines estimated from the temperature dependence. Thus, one can conclude that the local structure of the trapped excited state is essentially similar to that of the high-temperature phase within the experimental and/or analytical errors, although more amount of the high-temperature phase is obtainable with light irradiation rather than with heating.

## IV. CONCLUSIONS

The present work demonstrates that the XAFS spectroscopy was successfully applied to the local structure determination of a photoexcited state which is effectively trapped at low temperature. We have measured and analyzed the Fe and Co *K*-edge XAFS spectra of the photoexcited state of $Na_{0.4}Co_{1.3}Fe(CN)_6 \cdot 5H_2O$ at 36 K. Owing to detailed supplementary investigation on the temperature-dependence measurements which cover both the low- and high-temperature phases, the amount of the Co(III) ratios was determined quantitatively through the factor analysis of the XANES spectra. The local structure of the excited state was found by the EXAFS analysis to be identical with that of the high-temperature phase within the experimental/analytical errors. The Fe-C distance shows almost no change on light irradiation (1.92 Å before and after irradiation), while the average Co-N/O distance is noticeably elongated (1.94 and 2.08 Å before and after irradiation, respectively) due to the charge transfer from the $Fe^{II}$-CN-$Co^{III}$ configuration to $Fe^{III}$-CN-$Co^{II}$. It was also clarified much higher composition ratio of the high-temperature phase can be achieved by the visible-light irradiation than by thermal activation.

## ACKNOWLEDGMENTS

The authors are grateful for the financial support of a Grand-in-Aid for Scientific Research from the Ministry of Education in Japan (No. 10304059). The present work has been performed under the approval of Photon Factory Program Advisory Committee (PF-PAC No. 97G034).

[1] S. Ferlay, T. Mallah, R. Ouahés, P. Veillet, and M. Verdaguer, Nature (London) **378**, 701 (1995).
[2] O. Sato, T. Iyoda, A. Fujishima, and K. Hashimoto, Science **271**, 49 (1996).
[3] O. Sato, T. Iyoda, A. Fujishima, and K. Hashimoto, Science **272**, 704 (1996).
[4] O. Sato, Y. Einaga, T. Iyoda, A. Fujishima, and K. Hashimoto, J. Phys. Chem. B **101**, 3903 (1997).
[5] O. Sato *et al.* (unpublished).
[6] T. Yokoyama, T. Ohta, O. Sato, and K. Hashimoto, Phys. Rev. B **58**, 8257 (1998).
[7] M. Fernández-García, C. Márquez Alvarez, and G. L. Haller, J. Phys. Chem. **99**, 12 565 (1995).
[8] S. I. Zabinsky, J. J. Rehr, A. Ankudinov, R. C. Albers, and M. J. Eller, Phys. Rev. B **52**, 2995 (1995).
[9] M. Nomura (unpublished).
[10] M. Nomura and A. Koyama (unpublished).
[11] T. Yokoyama, H. Hamamatsu, and T. Ohta, EXAFSH Version 2.1 (The University of Tokyo, 1993).
[12] A. Frenkel, E. A. Stern, A. Voronel, M. Qian, and M. Newville, Phys. Rev. B **49**, 11 662 (1994).